Essential role of papillae flexibility in nectar capture by bees

Amandine Lechantre[a,b,c,1,2] (iD), Ayrton Draux[a,2], Hoa-Ai Béatrice Hua[d] (iD), Denis Michez[e] (iD), Pascal Damman[a] (iD), and Fabian Brau[d,3] (iD)

[a]Laboratoire Interfaces & Fluides Complexes, Université de Mons, B-7000 Mons, Belgium; [b]Laboratoire de Physique et Mécanique des Milieux Hétérogènes (PMMH), UMR 7636 of CNRS, École Supérieure de Physique et de Chimie Industrielles, 75005 Paris, France; [c]Laboratoire Matières et Systèmes Complexes (MSC), UMR 7057 of CNRS, Université de Paris, 75006 Paris, France; [d]Nonlinear Physical Chemistry Unit, Université libre de Bruxelles, 1050 Bruxelles, Belgium; and [e]Laboratoire de Zoologie, Université de Mons, B-7000 Mons, Belgium

Many bees possess a tongue resembling a brush composed of a central rod (glossa) covered by elongated papillae, which is dipped periodically into nectar to collect this primary source of energy. In vivo measurements show that the amount of nectar collected per lap remains essentially constant for sugar concentrations lower than 50% but drops significantly for a concentration around 70%. To understand this variation of the ingestion rate with the sugar content of nectar, we investigate the dynamics of fluid capture by *Bombus terrestris* as a model system. During the dipping process, the papillae, which initially adhere to the glossa, unfold when immersed in the nectar. Combining in vivo investigations, macroscopic experiments with flexible rods, and an elastoviscous theoretical model, we show that the capture mechanism is governed by the relaxation dynamics of the bent papillae, driven by their elastic recoil slowed down through viscous dissipation. At low sugar concentrations, the papillae completely open before the tongue retracts out of nectar and thus, fully contribute to the fluid capture. In contrast, at larger concentrations corresponding to the drop of the ingestion rate, the viscous dissipation strongly hinders the papillae opening, reducing considerably the amount of nectar captured. This study shows the crucial role of flexible papillae, whose aspect ratio determines the optimal nectar concentration, to understand quantitatively the capture of nectar by bees and how physics can shed some light on the degree of adaptation of a specific morphological trait.

bee | nectar capture | fluid–structure interaction | viscous dissipation

The ingestion of liquids to stay hydrated is an essential need for living organisms. Various natural strategies have emerged during the course of evolution to transport fluids. Large animals typically use gravity to drink low-viscosity fluids like water (human, birds) or use various methods to counteract gravity such as lapping [feline (1)], ladling [Canidae (2)], or active suction (Bovidae, Equidae). Small animals use instead viscous and capillary suction (butterflies, hummingbirds, etc.), dipping (bees, ants, bats, etc.), or contrasted wetting properties of their body (Namib desert beetle) to capture fluids (3, 4).

Some insects, birds, and small mammals hydrate and feed simultaneously by ingesting nectar. Capturing such a viscous fluid at small scales is a challenge that nectarivores have solved by developing various types of specialized tongues through natural selection leading to the propagation of favorable traits (5). The coevolution of bees and flowers is a well-known example of such mechanisms highlighted by the various shapes of the tongue observed among bee species in relation to the diversity in flower morphology (6). One intuitive example is the correlation between the corolla depth and the tongue length (7–10).

The relation between the nectar sugar concentration and the bees' tongue morphology is more subtle. Indeed, since the energy content of a given volume of nectar is proportional to its sugar concentration, flowers should a priori produce the sweetest possible nectar to attract bees interested by maximizing their energy intake. However, our in vivo measurements for *Bombus* show that very sweet nectar is not the best for bees. Fig. 1*A* shows images of a *Bombus terrestris* feeding on a sugar solution. The meniscus at the liquid–air interface moves in average at a constant speed, v_m, inside the capillary tube as the liquid is ingested by the *Bombus* and yields the ingestion rate $Q = v_m S_c$ where S_c is the area of the inner section of the capillary (Fig. 1*B* and *Materials and Methods*). The temporal evolution of the meniscus position $p(t)$ reveals, however, small periodic variations related to the periodic motion of the tongue from which the lapping rate T_L^{-1} is determined (Fig. 1 *B*, *Inset*). Repeating this experiment at various sugar concentrations, c_s, shows that the lapping rate is essentially constant (Fig. 1*C*) with a lapping time $T_L \simeq 0.2$ s in agreement with previous measurements on various bee species (11–13, 15–18). For each concentration considered, the ingestion rate is obtained and reported in Fig. 1*D* together with others found in the literature for other bee species (11, 14). Those results show that the ingestion rate of nectar remains essentially constant for sugar concentrations $c_s \lesssim 50\%$ but decreases significantly at 70%. As shown below, this implies that the energy intake rate is maximum around $c_s^\star \simeq 50$ to 60%. Therefore, there is no reason for plants visited by bees to produce nectar with $c_s > c_s^\star$. This may explain why the sugar concentration of flower nectar rarely exceeds 60% (25, 26).

Significance

Flowers provide the energy resources of bees. In a competitive world, we can hypothesize that flowers attract bees by producing very sweet nectar since it offers the greatest energetic rewards. However, the nectar sugar concentration rarely exceed 60%, and in vivo measurements show that bees capture nectar less efficiently beyond that limit. Here, we explain the physiological origin of this limit based on an elastoviscous mechanism. Most of bees collect the nectar with tongues covered by elongated papillae that open when immersed in a fluid, the opening dynamics determining the amount of nectar collected per lap. At very large sugar concentrations, we found that viscous forces impede the full opening of papillae, reducing the amount of nectar collected.
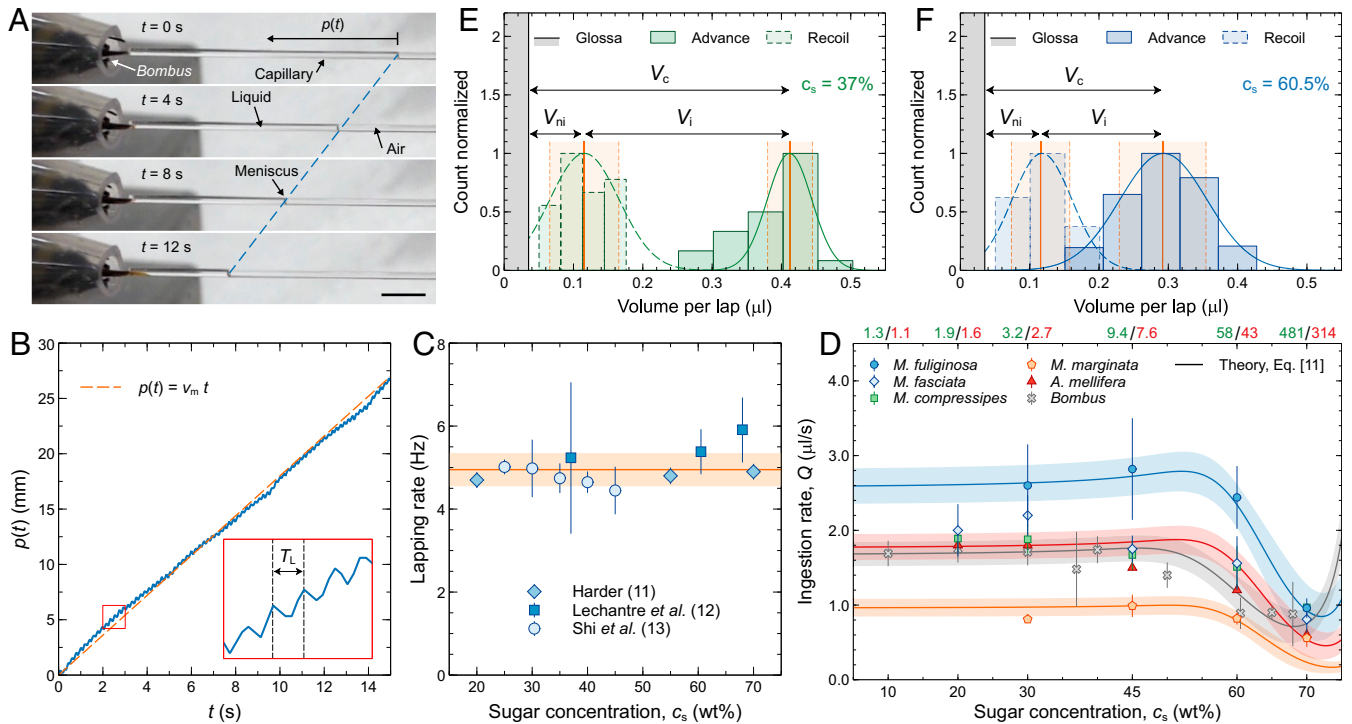
APPLIED PHYSICAL SCIENCES

Fig. 1. (*A*) Snapshots of a feeding process with a 60.5% sugar solution ($\mu = 0.065$ Pa s) (Movie S1). (Scale bar: 5 mm.) (*B*) Evolution of the position $p(t)$ of the liquid–air interface as a function of time during the feeding process shown in *A*. (*Inset*) Evolution of $p(t)$ between $t = 2$ s and $t = 3$ s. (*C*) Lapping rate as a function of the sugar concentration c_s at 20°C (11–13). The shaded area highlights the range $T_L^{-1} = (4.95 \pm 0.40)$ Hz. (*D*) Comparison between the theoretical ingestion rate Q (Eq. **11**) and in vivo measurements for different species of *Melipona*, *Apis* (14), and *Bombus* (11, 12) as a function of the sugar concentration. The viscosity in millipascals second at 20 °C/30°C is also indicated on the top axis. The parameter values used are $T_L = 2T_R = (0.20 \pm 0.02)$ s (11–13, 15–18), $d_m = L \sin(\pi/4)$ (16, 18–20), and $E = (1.1 \pm 0.1)$ MPa for all species; $R_G = (50 \pm 5)$ μm, $R = (2.9 \pm 0.1)$ μm, and $L = (170 \pm 5)$ μm (19, 21) for *Melipona* and *Apis*; and $R_G = (95 \pm 5)$ μm, $R = (2.1 \pm 0.1)$ μm, and $L = (135 \pm 5)$ μm for *Bombus*. The value of E is comparable with the Young modulus of the tip of the adhesive tarsal setae of beetles (22, 23) or of the lepidopteran proboscis (24) (discussion is in *SI Appendix*). The small variation of the nectar density ρ_l with μ is negligible due to the small exponent in Eq. 10, and $\rho_l = (1,175 \pm 175)$ kg/m^3 is used (*SI Appendix*). The immersion length, L_I, of the tongue is varied proportionally to the tongue length, L_T, for each species [$L_I \simeq (0.6\,L_T - 1)$ mm]: $L_I = 3.2 \pm 0.1$ mm (*Melipona fuliginosa*, $L_T = 7.0$ mm), $L_I = 2.2 \pm 0.1$ mm (*Apis mellifera*, $L_T = 5.4$ mm), $L_I = 2.0 \pm 0.1$ mm (*Bombus*, $L_T = 5.0$ mm), and $L_I = 1.2 \pm 0.1$ mm (*Melipona marginata*, $L_T = 3.8$ mm) (12, 14). The theoretical curves for *Melipona fasciata* and *Melipona compressipes* ($L_T = 5.9$ mm) are close to the one for *A. mellifera* and are not shown for clarity. The shaded areas show the regions spanned by the theoretical curves when the parameters are varied within their error bars. (*E* and *F*) Distributions of the volumes per lap associated with the advances and recoils of the meniscus seen in *B*, *Inset* for $c_s = 37\%$ and 62 laps (*E*) and $c_s = 60.5\%$ and 261 laps (*F*). The distributions are fitted by normal distributions, and the orange shaded areas extend over one SD around the mean value.

Two origins can be considered to explain the drop in ingestion rate observed for a concentration near 70%. It could be related either to the difficulty to swallow nectar when its viscosity (c_s) increases or to an intrinsic limitation of the capture mechanisms itself (i.e., the tongue captures less nectar per lap as c_s increases). Interestingly, the small periodic oscillations of the meniscus position $p(t)$ seen in Fig. 1*B* allow us to discriminate between both explanations. As the tongue enters the liquid, the meniscus recoils due to the added extra volume composed of the tongue and the remaining noningested fluid (V_{ni}). When the tongue exits the capillary, in contrast, the meniscus advances due to the lost volume related to the tongue and the captured fluid (V_c) removed from the capillary. The amount of ingested nectar is then given by $V_i = V_c - V_{ni}$. The distributions of V_c and V_{ni} for two values of sugar concentration c_s are shown in Fig. 1 *E* and *F*. Clearly, V_{ni} is insensitive to variations in c_s, whereas V_c decreases as c_s increases. These results indicate that the drop in the volume ingested per lap, V_i, is due to a decrease of the amount of nectar captured by the tongue when c_s increases.

The loss of efficiency of the bees' tongues in capturing very sweet nectar should then be related to its fine structure, which is ignored in previous models (27). The viscous dipping of smooth rods does not account for the drop in ingestion rate. Indeed, since the bees' lapping period, T_L, is essentially constant, the thickness of the liquid layer covering a bare tongue when it retracts out of nectar should increase monotonically with its viscosity and thus, with its sugar concentration, according to the Landau–Levich–Derjaguin (LLD) mechanism (28–31).

The tongue of a bee is composed of a glossa of radius $R_G \sim (50 - 100)$ μm decorated by solid elongated papillae of length $L \sim (100 - 200)$ μm and radius $R \sim (2 - 3)$ μm (12, 15–21, 32–35) (*SI Appendix*). There are approximately 2,500 papillae per square millimeter so that the average distance between them is about $8R$ (15, 17, 19, 21, 33, 34). This density is thus quite small compared with the setae density of some arthropods such as fly (*Calliphora erythrocephala*, 1.5×10^5/mm^2), bug (*Rhodnius*, 2×10^5/mm^2), or spider (*Cupiennius salei*, 2.1×10^6/mm^2) (36). During the drinking process, the papillae initially adhere to the glossa due to capillary forces and open when immersed in the nectar (Movie S1). Fig. 2 *A* and *B* shows indeed that capillary forces are strong enough to keep the papillae bent in contact with the glossa. This elastocapillary effect is also observed when bees feed on dry sugar since the papillae open well after the protrusion phase and only when enough saliva is secreted to dissolve the sugar (37).

To determine the role of the papillae in the nectar capture, we analyze their in vivo dynamics recorded with an optical microscope fitted with a high-speed camera for *B. terrestris* (*Materials*
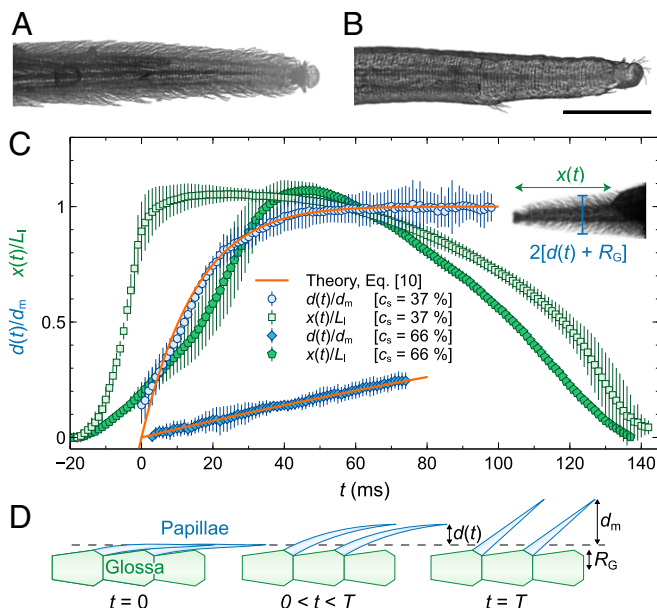
Fig. 2. (*A* and *B*) Optical microscopy photography of a *B. terrestris* tongue. The papillae are fully open when the tongue is immersed in water (*A*), whereas they adhere to the glossa due to capillary forces after the tongue is withdrawn from the liquid (*B*). (Scale bar: 500 μm.) (*C*) Evolution of the rescaled distances $x(t)/L_1$ and $d(t)/d_m$ as a function of time for two values of c_s for *B. terrestris*. $L_1 \simeq 2$ mm is the immersion length of the tongue, and $d_m \simeq 95$ μm is the maximum extension of the papillae. $d(t)$ is the average of measurements performed at four distances from the tip of the tongue (500, 750, 1,000, and 1,250 μm) (*SI Appendix* has raw data). The theoretical curves [10] are shown with $\rho_1 = 1,150$ kg/m³, $\mu = 5$, and 200 mPa s (20°C) together with *E*, *R*, *L*, and d_m used in Fig. 1*D* for *Bombus*. (*D*) Schematic of the papillae relaxation dynamics.

and Methods). The temporal variations of the position of the tongue tip with respect to the galea, $x(t)$, and of the distance $d(t)$ between the tip of the papillae and the glossa during the capture process are shown in Fig. 2*C*. At low sugar concentration, c_s, the papillae open to reach a maximum extension $d_m \simeq 95$ μm before the tongue completely retracts out of the liquid and thus, fully contribute to the nectar capture. In contrast, at a larger c_s for which a drop of the ingestion rate is observed, the papillae do not have the time to completely open during a protraction–retraction cycle due to the viscous dissipation impacting both their dynamics and their benefits in collecting nectar. The temporal evolution of $x(t)$ shows that the protraction of the tongue is impacted by the nectar viscosity. However, in both cases shown in Fig. 2*C*, the total immersion length of the tongue, $L_1 \simeq 2$ mm, and the retraction time, $T_R \simeq 0.1$ s, are similar in agreement with the observation that the lapping frequency is essentially insensitive to the nectar viscosity (11–13). These observations further confirm that bees are able to adjust the retraction force to the nectar viscosity (12).

To mimic the opening dynamics of a single papilla, we consider the unbending dynamics of a deflected flexible rod in a viscous fluid. A rod of length L, radius R, Young modulus E, and density ρ_s is clamped at one extremity and deflected at its free end while immersed in a liquid of viscosity μ and density ρ_1 (Fig. 3*A* and *Materials and Methods*). By varying systematically these control parameters, we show the existence of two regimes: under- and overdamped, separated by a transient stage. Each regime is characterized by distinct scaling for their relaxation times, T, defined as the time at which the rod passes through its rest position for the first time (Fig. 3*B*). For the underdamped regime, where the rod oscillates around its equilibrium position, T is pro-

portional to the oscillation period, whereas in the overdamped regime, there is no oscillation, and T is the time needed for the rod to return to equilibrium.

The theoretical analysis of the rod relaxation dynamics requires to couple the Navier–Stokes and elasticity equations and is unfortunately intractable. Therefore, we propose to decouple the fluid and the rod equations by adding an effective viscous force to the dynamical beam equation (38), which then reads

$$\bar{\rho}_{sl}\, \partial_t^2 w(x,t) = -B\, \partial_x^4 w(x,t) - F_\mu, \qquad [1]$$

where $w(x,t)$ is the transverse displacement of the rod along the y axis, $B = \pi E R^4/4$ is the bending modulus of a cylindrical rod, $\bar{\rho}_{sl} = (\rho_s + \rho_1)S \equiv \rho_{sl}S$ is the linear mass density of the rod supplemented by the linear mass of the displaced fluid (39), and $S = \pi R^2$ is the section area of the rod.

The expression of the viscous force per unit length, F_μ, is a priori complicated since it depends on the local fluid velocity, which varies in space and time. Here, we propose to use the viscous drag experienced by a rigid cylinder moving at a constant speed perpendicular to its symmetry axis and obtained by solving the Stokes equations with the Oseen's correction (40):

$$F_\mu = S_g \frac{4\pi\mu\, v}{c - \ln(v/v_c)}, \qquad v_c = \frac{4\mu}{\rho_1\, R}, \qquad [2]$$

where $v = |\partial_t w|$ is the rod velocity, S_g is the sign of $\partial_t w$ so that the viscous force is always acting against the rod motion, and $c = 1/2 - \gamma_E$ where $\gamma_E \simeq 0.577$ is the Euler constant. Notice that the data reported in Figs. 1*D*, 2*C*, and 3*B* are obtained with Newtonian fluids [at least up to $c_s = 85\%$ for sucrose solutions (41–43)].

Since Eqs. **1** and **2** depend on numerous parameters, it is useful to consider its adimensionalized form. Using $\bar{w} = w/\ell$, $\bar{x} = x/L$, and $\bar{t} = t/\tau$, where τ and ℓ are defined as

$$\tau = \rho_{sl}R^2/4\mu \quad \text{and} \quad \ell = v_c\tau, \qquad [3]$$

we obtain the adimensionalized form of Eq. **1**:

$$\partial_{\bar{t}}^2 \bar{w}(\bar{x},\bar{t}) = -k\, \partial_{\bar{x}}^4 \bar{w}(\bar{x},\bar{t}) - \bar{F}_\mu, \qquad k = \frac{E\rho_{sl}R^6}{64\,\mu^2 L^4}, \qquad [4]$$

where $\bar{F}_\mu = S_g \bar{v}/[c - \ln \bar{v}]$ and $\bar{v} = v/v_c = |\partial_{\bar{t}}\bar{w}|$. Eq. **4** can be solved numerically by imposing that the deflected rod is clamped at $\bar{x} = 0$, free at $\bar{x} = 1$, and released without initial velocity as in the experiments. The relaxation times, T/τ, obtained from the numerical solutions are in good agreement with the experimental data spanning 12 orders of magnitude for k (Fig. 3*B*).

The relaxation dynamics of the bee's papillae occur at low values of the ratio v/v_c, vide infra. To gain some analytical insights into the relaxation dynamics in this regime, we notice that, when $v/v_c \lesssim 10^{-3}$, the evolution of $\bar{F}_\mu$ with the velocity is described in very good approximation by a power law (Fig. 3*C*):

$$\bar{F}_\mu = S_g\, \beta\, \bar{v}^{11/10}, \qquad \beta = 0.288. \qquad [5]$$

The viscous force is thus not proportional to the rod velocity in agreement with the observed nonexponential relaxation dynamics reported in Fig. 3*D*. Notice, however, that to describe the evolution of the ingestion rate as a function of the sugar concentration shown in Fig. 1*D*, a linear approximation for the viscous force could also be used. The difference between the two descriptions is smaller than the typical uncertainty on the in vivo data (*SI Appendix*).

In the overdamped regime, the rod inertia is negligible, and since there is no oscillation, the rod velocity is negative such that
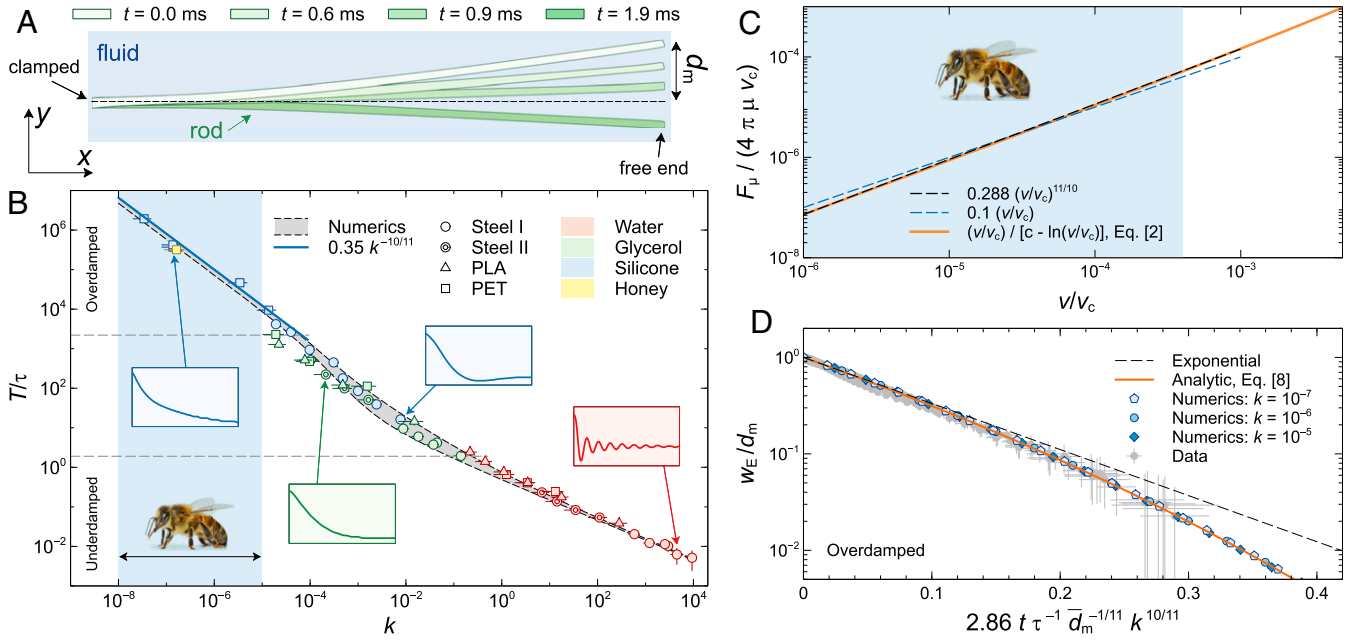
Lechantre et al.
Essential role of papillae flexibility in nectar capture by bees

PNAS | 3 of 7
https://doi.org/10.1073/pnas.2025513118

Fig. 3. (*A*) Snapshots of a deflected stainless steel rod of length $L = 54$ mm oscillating in water at various times as indicated. The horizontal dashed line indicates the equilibrium position. (*B*) Evolution of the experimental rescaled relaxation time T/τ as a function of the control parameter k (Eq. **4**) for various types of rods and fluids. The gray shaded area shows the variation of the theoretical curve, obtained by solving numerically Eq. **4**, as the rescaled imposed transverse displacement of the tip of the rod, $\bar{d}_m$, is varied within its experimental range ($0.4 \leq \bar{d}_m \leq 10.5$). (*Insets*) Positions of the tip of the rod as a function of time for some representative cases. (*C*) Evolution of the rescaled viscous force, $\bar{F}_\mu = F_\mu/(4\pi\mu v_c)$ (Eq. **2**), as a function of the rescaled velocity, $\bar{v} = v/v_c$ (solid orange curve) together with a power law approximation for $\bar{v} \leq 10^{-3}$ (dashed black curve). (*D*) Evolution of the rescaled position of the tip of the rod, w_E/d_m, as a function of a rescaled time for the overdamped regime. Data obtained by solving numerically Eqs. **4** and **5** are compared with the experimental data and the asymptotic theoretical curve [8]. An exponential decay arising from a viscous force varying linearly with v is shown for comparison.

$|\partial_{\bar{t}} \bar{w}| = -\partial_{\bar{t}} \bar{w}$ and $S_g = -1$. Therefore, Eq. **4** with the viscous force [5] becomes

$$k\,\partial_{\bar{x}}^4 \bar{w}(\bar{x}, \bar{t}) = \beta\,[-\partial_{\bar{t}} \bar{w}(\bar{x}, \bar{t})]^{11/10}. \qquad [6]$$

Using the separation of variables, $\bar{w}(\bar{x}, \bar{t}) = \bar{w}_E(\bar{t})g(\bar{x})$ where $\bar{w}_E(\bar{t})$ describes the temporal evolution of the tip of the rod, Eq. **6** reduces to two ordinary differential equations:

$$\dot{\bar{w}}_E = -\,[\eta\, k/\beta]^{10/11}\,\bar{w}_E^{10/11}, \quad \bar{w}_E(0) = \bar{d}_m, \qquad [7a]$$

$$g'''' = \eta\, g^{11/10}, \quad g(0) = g'(0) = g''(1) = g'''(1) = 0, \qquad [7b]$$

where η is the separation constant, $d_m = \ell\,\bar{d}_m$ is the imposed transverse displacement of the tip of the rod, and dot and prime indicate time and spatial derivatives, respectively. The boundary conditions indicate that the rod is clamped at $\bar{x} = 0$ and free at $\bar{x} = 1$ (Fig. 3*A*). The nonlinear eigenvalue Eq. **7b** can be solved numerically with $g(1) = 1$ [i.e., $\bar{w}(1, 0) = \bar{d}_m$], so that $\eta \simeq 12.803$. The temporal evolution of the position of the tip of the rod is then obtained by integrating Eq. **7a**:

$$\frac{\bar{w}_E(\bar{t})}{\bar{d}_m} = \left[1 - 2.86\,\frac{k^{10/11}}{\bar{d}_m^{1/11}}\,\bar{t}\right]^{11}. \qquad [8]$$

Fig. 3*D* shows that, when time is properly rescaled, the numerical solutions of Eqs. **4** and **5** at small k and the experimental data in overdamped regime collapse on the asymptotic expression [8]. The latter implies that the relaxation time T at which the rod returns to equilibrium (i.e., $w_E = 0$) is given by

$$T/\tau = 0.35\,\bar{d}_m^{1/11}\,k^{-10/11} \simeq 0.35\,k^{-10/11}. \qquad [9]$$

Fig. 3*B* shows the good agreement between the asymptotic expression [9] and experimental data.

By measuring the relaxation time $T \gtrsim 0.06$ s of the papillae from in vivo measurements (Fig. 2*C*) (16, 19, 20), for $\mu = 5$ mPa s and using the radius R and the length L of the papillae reported in Fig. 1*D*, we find $v/v_c \simeq d_m/(v_c T) \lesssim 10^{-4}$ so that Eq. **5** is valid. Notice that, since $v/v_c \sim \mu^{-1}$, this ratio is even smaller at larger viscosity. The temporal evolution of the distance $d(t) = d_m - w_E(t)$ between the tip of the papillae and the glossa is thus obtained from Eq. **8**:

$$\frac{d(t)}{d_m} = 1 - \left[1 - \frac{t}{T}\right]^{11}, \quad T = 4.35\left[\frac{\mu^{10}\,d_m}{\bar{E}^{10}\,v_c}\right]^{1/11}, \qquad [10]$$

where Eq. **9** has been written in a more convenient form with $\bar{E} = ER^4/L^4$ an effective rod stiffness. Eq. **10** describes the relaxation dynamics of the papillae as shown schematically in Fig. 2*D*. At $t = 0$, $d(0) = 0$, and the papillae adhere to the glossa; at $t = T$, $d(T) = d_m$, and the papillae are fully open. Using the parameter values reported in Fig. 1*D* for *Bombus*, the temporal evolution of $d(t)/d_m$ is found to be in very good quantitative agreement with in vivo measurements of the papillae relaxation dynamics (Fig. 2*C*).

A model for the nectar capture by bees taking into account the relaxation dynamics of the papillae can now be developed. Since the distance between the papillae is large compared with their radius ($\sim 8R$) and the Reynolds number is very low ($\mathrm{Re} \sim v/v_c \lesssim 10^{-4}$), the interference between drag flows generated by adjacent papillae can be neglected (44, 45).

As shown in Fig. 1, bees collect nectar by quickly protracting and retracting their tongue with a constant lapping period, which is the sum of the protraction time, of the retraction time, and of the nectar unloading time. The volume of nectar collected when the tongue retracts out of nectar at $t = T_R \simeq T_L/2$ is the sum of
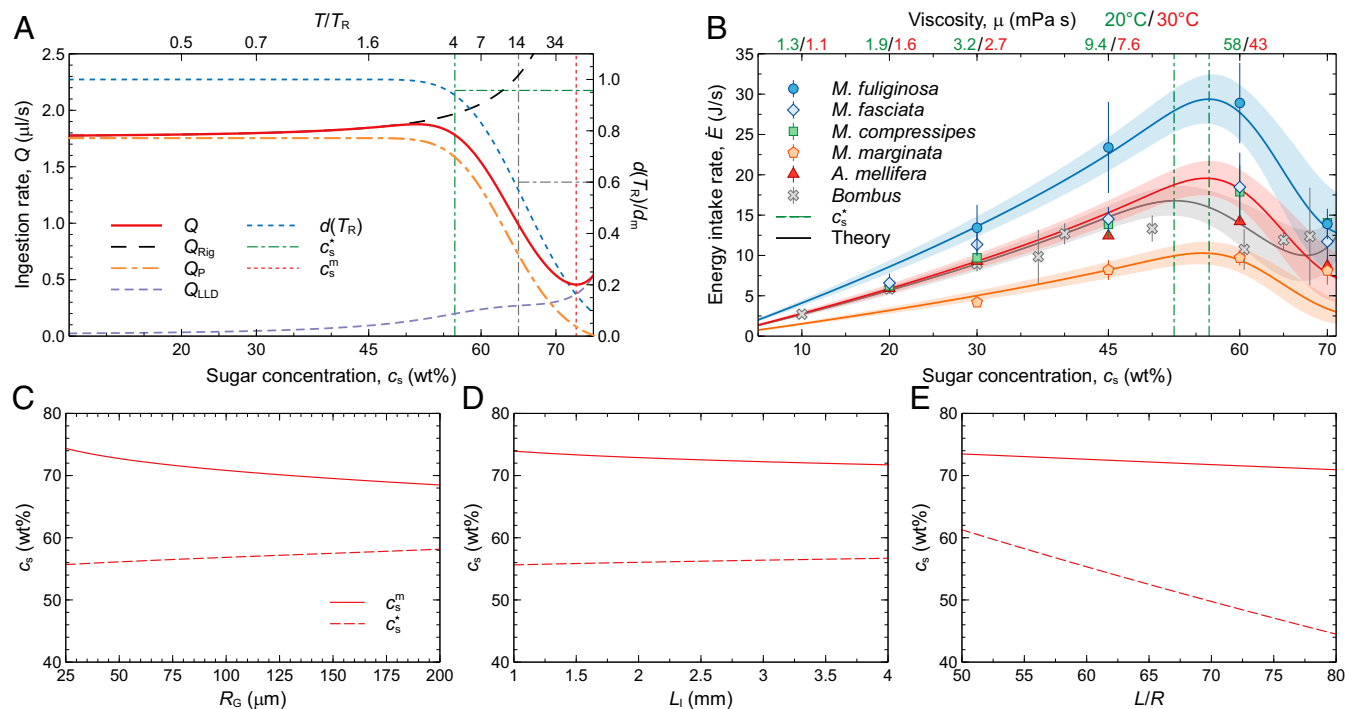
Fig. 4. (*A*) Evolution of the ingestion rate Q as a function of the sugar concentration for *A. mellifera* as shown in Fig. 1*D* together with the contribution Q_P of the papillae and of the dragged film, Q_{LLD}. The ingestion rate for rigid papillae, Eq. **12**, is shown for comparison. The evolution with the sugar concentration c_s of the normalized distance between the tip of the papillae and the glossa at $t = T_R$ [i.e., $d(T_R)/d_m$] is shown on the right axis. The values of this ratio at the optimal value $c_s = c_s^\star$ and at $c_s = 65\%$ are highlighted. The values of the ratio T/T_R at some particular sugar concentrations are shown on the top axis. The value c_s^m of the sugar concentration at which Q is minimum is also shown. (*B*) Evolution of the energy intake rate, $\dot{E}$, as a function of the sugar concentration for several bee species obtained from Eqs. **11** and **13** with the same parameter values as those used in Fig. 1*D*. The shaded areas show the regions spanned by the theoretical curves when the parameters are varied within their error bars. The vertical dashed lines indicate the concentrations at which $\dot{E}$ is maximum for *Melipona*, *Apis*, and *Bombus* species. The symbols represent data obtained by using Eq. **13** together with the in vivo measurements of Q shown in Fig. 1*D*. (*C*–*E*) Evolution of the concentration c_s^m, at which the ingestion rate Q is minimum, and of the concentration $c_s^\star$, at which the energy intake rate $\dot{E}$ is maximum, as a function of the glossa radius, R_G (*C*), of the immersion length L_I (*D*), and of the papillae aspect ratio L/R (*E*). The value of the parameters reported in Fig. 1*D* for *A. mellifera* are used, and R_G, L_I and L/R are varied separately.

the volume trapped by the papillae and the volume dragged by an LLD mechanism (28–31). The former is delimited by the glossa of radius R_G and the tip of the papillae located at a distance $d(T_R)$ from the glossa (Eq. **10**). This volume per unit of time, Q_P, reads $Q_P = \pi v_R[\tilde{R}_G^2 - R_G^2]$, where $\tilde{R}_G = R_G + d(T_R)$ and $v_R = L_I/T_R$ is the average retraction velocity with L_I the immersed length of the tongue. The total volume of the immersed papillae is negligible (*SI Appendix*). The volume dragged per unit of time by the hairy structure through an LLD mechanism is given by $Q_{LLD} = \pi v_R[(\tilde{R}_G + h)^2 - \tilde{R}_G^2]$, where $h = 1.34\,\tilde{R}_G\,\mathrm{Ca}^{2/3}$ is the thickness of the film of nectar dragged (30, 31), $\mathrm{Ca} = \mu v_R/\gamma$ is the capillary number, and $\gamma \simeq 0.074$ N/m is the surface tension that does not vary significantly with c_s (46). The total volume of nectar collected per unit of time, $Q = Q_P + Q_{LLD}$, is thus finally given by

$$Q = \pi v_R \left[[R_G + d(T_R)]^2 \left[1 + 1.34\,\mathrm{Ca}^{2/3} \right]^2 - R_G^2 \right], \qquad \textbf{[11]}$$

with $d(T_R)$ given by Eq. **10**.

At low c_s, the papillae relaxation time, T, is smaller than the retraction time, T_R, so that $d(T_R) = d_m$. The ingestion rate is then essentially constant, $Q \simeq \pi v_R[(R_G + d_m)^2 - R_G^2]$, in agreement with the in vivo measurements reported in Fig. 1*D*. The volume captured in this case is thus essentially equal to the volume trapped by the papillae, $Q \simeq Q_P$, since the thickness h of the dragged film is negligible ($\mathrm{Ca} \ll 1$). At sufficiently large sugar concentration, $c_s \gtrsim 50\%$, T becomes significantly larger than T_R.

The papillae do not have enough time to fully open, $d(T_R) < d_m$, when the tongue retracts out of nectar, which impacts the ingestion rate (Fig. 4*A*). Using the measured physiological parameters of *B. terrestris* (Fig. 1*D* and *SI Appendix*), Eq. **11** describes well the in vivo data reported in Fig. 1*D*. A similar quantitative agreement is obtained for *Apis mellifera* when their physiological parameters reported in the literature are used. Fig. 1*D* reveals also a correlation between the ingestion rate, Q, and the total length of the tongue, L_T (10). Using the values of L_I reported in Fig. 1*D* while keeping all of the other parameters unchanged, Eq. **11** also describes well the data for *Melipona* species.

Fig. 4*A* shows that, for moderate sugar concentrations, the volume of the film dragged through an LLD mechanism is negligible compared with the volume trapped by the papillae, whereas it becomes dominant at large c_s. Indeed, the sharp increase in viscosity observed for $c_s \simeq 70\%$ impacts strongly the relaxation dynamics of the papillae, which remain in close contact with the glossa during retraction (i.e., the fine structure of the tongue can no longer helps in collecting nectar). Notice that for rigid microstructures mimicking the papillae (12), $d(T_R) = d_m$ for all c_s so that Eq. **11** becomes

$$Q_{Rig} = \pi v_R \left[[R_G + d_m]^2 \left[1 + 1.34\,\mathrm{Ca}^{2/3} \right]^2 - R_G^2 \right]. \qquad \textbf{[12]}$$

Eq. **12** and Fig. 4*A* show a continuous increase of Q_{Rig} with c_s. The sharp drop observed for Q at large c_s, which is well described by Eq. **11**, is therefore a clear signature of the papillae flexibility.
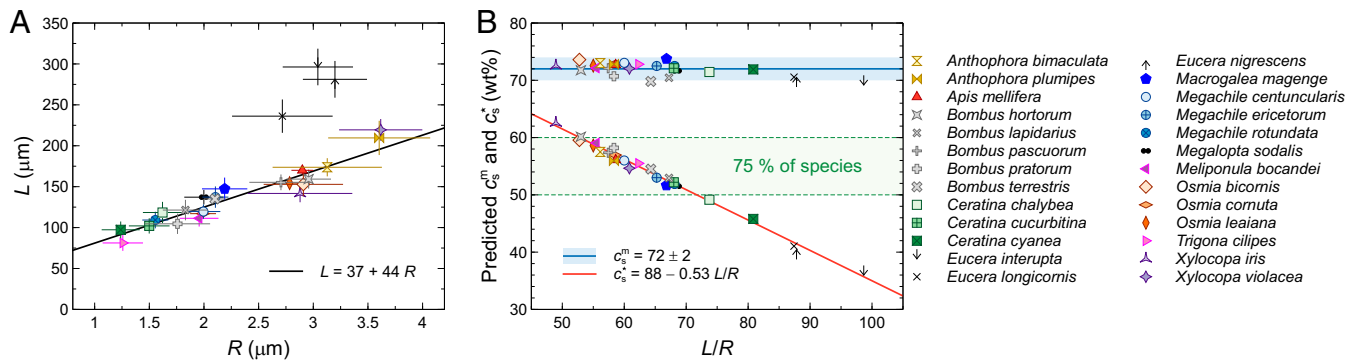
APPLIED PHYSICAL SCIENCES

Fig. 5. (*A*) Evolution of the papillae length L as a function of their radius R for 26 bee species measured on SEM images (*SI Appendix*, Table S1). The solid line highlights a linear relationship where the coefficients are given for L and R measured in micrometers. (*B*) Evolution of the sugar concentration c_s^m, at which the ingestion rate Q is minimum, and of the sugar concentration $c_s^\star$, at which the energy intake rate $\dot{E}$ is maximum, as a function of the ratio L/R for the same bee species. These two concentrations have been computed from Eqs. **11** and **13** using the values of R_G, L, and R associated with each species (*A* and *SI Appendix*, Table S1) together with the values of T_L, T_R, d_m, E, and ρ_l used in Fig. 1*D* for all species. Since the influence of L_I on those concentrations is very limited (Fig. 4*D*) c_s^m and $c_s^\star$ are averaged for L_I varying between 1 and 4 mm (*SI Appendix*, Table S1). c_s^m is essentially constant, whereas $c_s^\star$ varies linearly with L/R in good approximation.

After the ingestion rate is known, the energy intake rate, $\dot{E}$, can be easily computed using

$$\dot{E}(c_s) = \sigma\, Q(c_s)\, \rho_l(c_s)\, c_s,\qquad\qquad \textbf{[13]}$$

where $\sigma = 15.48$ kJ/g is the energy content per unit mass of sugar (11) and Q is given by Eq. **11**. The dependence of the nectar mass density on the sugar concentration is here taken into account (*SI Appendix*, Eq. **S17**) since $\dot{E}$ varies linearly with ρ_l in contrast to Q, which depends very weakly on this quantity. Fig. 4*B* shows that $\dot{E}$ is maximum at $c_s^\star \simeq 56\%$ for *Melipona* and *Apis* species and at $c_s^\star \simeq 53\%$ for *Bombus* in agreement with values reported previously (11, 14). Fig. 4*A* shows that the papillae are still open at about 95% of their full erection at those optimal concentrations when the tongue is withdrawn from the nectar [i.e., $d(T_R)/d_m \simeq 0.95$]. However, the ratio $d(T_R)/d_m$ drops quickly above these optimal concentrations. For example, the papillae are only open at 60% when $c_s = 65\%$.

Fig. 4 *A* and *B* shows the existence of two characteristic concentrations: c_s^m at which the ingestion rate Q is minimum and $c_s^\star$ at which the energy intake rate is maximum. The variations of these concentrations with respect to changes in the tongue morphology can be studied by varying the radius of the glossa R_G, the immersion length L_I, and the papillae aspect ratio L/R in the model. As illustrated in Fig. 4 *C–E*, the elastoviscous model shows that the concentration c_s^m is rather insensitive to the values of R_G, L_I, and L/R. However, the aspect ratio L/R has a significant impact on the concentration $c_s^\star$, whereas R_G and L_I have a very limited influence. Therefore, the drop in ingestion rate Q appears to be universal and should occur for most bee species at a similar value, close to 70% in sugar concentration, whereas the optimal concentration could vary with the bee species if the ratio L/R is not constant.

To gain a real insight into the possible variation of c_s^m and $c_s^\star$ among bees, we have measured R_G, L, and R on scanning electron microscopy (SEM) images for 24 additional long-tongued bee species from different genera distributed in Europe, Africa, and South America (*SI Appendix*). Fig. 5*A* shows that L increases linearly with R for all species except the *Eucera* species, which are characterized by more slender papillae. The values of these parameters are then used with Eqs. **10** and **11** to compute c_s^m and $c_s^\star$ as a function of the papillae aspect ratio L/R (Fig. 5*B*). As expected, the value of c_s^m is essentially constant, whereas $c_s^\star$ varies linearly with L/R. Such a simple relation can be use-

ful to estimate the optimal sugar concentration for various bee species. Nevertheless, since L/R varies between 50 and 70 for most species, the variation of $c_s^\star$ is moderate: $c_s^\star = (55 \pm 5)$ % for 75% of the species analyzed. This physiological limit of the bees' tongues may explain why the sugar concentration in nectar offered by flowers rarely exceeds 60% (25, 26). The observed adequacy of the physiological limit for bees and the maximum sugar concentration in flowers' nectar is probably not fortuitous and could be another example of the coevolution of connected species.

The present study explains the role of the papillae in the feeding process for bees. At low sugar concentration, the amount of nectar collected per unit time is essentially constant and controlled by the size of the tongue (i.e., the immersion length L_I and the glossa radius R_G) and by the length L of the papillae. As intuitively expected, larger bees collect more nectar per lap than smaller bees since the proboscis length increases essentially linearly with the body size (47). However, combined in vivo measurements and theoretical model show that the physiological limit for the nectar capture for various bee species is around 70% in sugar concentration. This limit is directly determined by the flexibility of the papillae and its associated relaxation time. Unexpectedly, this parameter discarded in most previous studies finally appears to be a crucial ingredient.

Materials and Methods

B. terrestris from the Biobest firm were used for the in vivo experiments. The colony was kept at the temperature of 27°C and humidity of 65 to 70%. They were fed every 2 d with pollen candies, and a sweet solution imitating the nectar (Biogluc pink) is provided to them ad libitum.

Ingestion Rate. Before beginning the observation of the drinking process, bumblebees were starved at the room temperature in the dark from 2 to 4 h. A bumblebee was then transferred into a centrifuge tube of 15 mL with a 4-mm hole at the tip. After a habituation phase of 3 min, the extension of the proboscis was motivated by presenting a drop of a solution of diluted honey. Finally, a capillary tube with an inner diameter $D_c = 0.8$ mm containing a sweet solution of known sugar concentration (or equivalently, viscosity) was presented to the bumblebee. The inner diameter is similar to the nectar tube width of some plants visited by *Bombus* (48, 49). The experiments were recorded by a camera Logitech C920 at 30 frames per second (Movie S1). The position $p(t)$ of the meniscus at the liquid–air interface was measured as a function of time, and the ingestion rate was obtained from $Q(t) = \pi D_c^2 v_m(t)/4$, where $v_m(t) = dp(t)/dt$ is the velocity of the meniscus. Since $p(t) \sim t$, v_m and Q are constant.

6 of 7 | **PNAS**
https://doi.org/10.1073/pnas.2025513118

Lechantre et al.
Essential role of papillae flexibility in nectar capture by bees

Relaxation Dynamics of Papillae. Bumblebees were starved from 1 to 2 h before beginning the experiment. A bumblebee was then transferred into a centrifuge tube of 50 mL with a 5-mm hole at the tip where it underwent a habituation phase of 3 min. A sweet solution of known viscosity was placed between two microscope slides spaced by a distance of 1 mm and was presented to the bumblebee. The capture dynamics were recorded under a binocular (Leica MZ16) fitted with a Photron Fastcam Mini AX200 operating at 1,000 frames per second with a 1,024 × 1,024-pixel resolution (Movie S1). The distance $x(t)$ between the tip of the tongue and the galea and the distance $d(t)$ between the tip of the papillae and the glossa were measured on each recorded image as detailed in *SI Appendix*.

Relaxation Dynamics of Rods. Rods made of various materials (steel, polylactide, and polyethylene terephthalate) with length 1.1 cm $\leq L \leq$ 9.0 cm, radius 0.15 mm $\leq R \leq$ 0.4 mm, Young modulus 5 GPa $\leq E \leq$ 165 GPa, and density 1,400 kg/m³ $\leq \rho_s \leq$ 8,300 kg/m³ were clamped at one extremity and deflected at their free end while immersed in various liquids (water, glycerol, and silicone oil from FungiLab) with viscosity 10^{-3} Pa s $\leq \mu \leq$ 10 Pa s and density 950 kg/m³ $\leq \rho_l \leq$ 1,100 kg/m³. The size of the fluid container is 32 × 115 × 60 mm³. The bending and Young moduli have been determined from the profile of the rods bent by a known force applied at their free end. The densities of both solids and liquids have been obtained by weighing a known volume of materials.

The rod was bent by manually displacing its free end by a distance 0.73 mm $\leq d_m \leq$ 4.9 mm depending on the rod length and radius. The initial displacement of the tip of the rod was small with respect to its length, $d_m/L \ll 1$, but large with respect to its radius, $d_m/R \gg 1$. After the free end was released, the motion of the rod was recorded by a Photron Fastcam SA3 high-speed camera operating at 1,000 to 5,000 frames per second until the rod returned to its horizontal equilibrium position. The relaxation dynamics always occur in the plane of the bent rod since recording its motion from different angles did not reveal any lateral deviation of the rod.

Propagation of Uncertainty. The uncertainty, δf, on a quantity $f(x_1, x_2, \dots)$ obtained from the combination of several other quantities x_i with uncertainty δx_i, like Q or T, was computed using the following relation:

$$(\delta f)^2 = \sum_i (\partial f/\partial x_i)^2 (\delta x_i)^2.$$

Data Availability. All study data are included in the article and/or supporting information.

1. P. M. Reis, S. Jung, J. M. Aristoff, R. Stocker, How cats lap: Water uptake by *Felis catus*. *Science* **330**, 1231–1234 (2010).
2. A. W. Crompton, C. Musinsk, How dogs lap: Ingestion and intraoral transport in *Canis familiaris*. *Biol. Lett.* **7**, 882–884 (2011).
3. W. Kim, J. W. M. Bush, Natural drinking strategies. *J. Fluid Mech.* **705**, 7–25 (2012).
4. A. R. Parker, C. R. Lawrence, Water capture by a desert beetle. *Nature* **414**, 33–34 (2001).
5. H. W. Krenn, *Insect Mouthparts* (Springer Nature Switzerland AG, Cham, Switzerland, 2019).
6. C. D. Michener, *The Bees of the World* (The Johns Hopkins University Press, Baltimore, MD, ed. 2, 2007).
7. A. D. Brian, Differences in the flowers visited by four species of bumble-bees and their causes. *J. Anim. Ecol.* **26**, 71–98 (1957).
8. I. Teräs, The honeybee's protrusible glossa is a compliant mechanism. *Ann. Zool. Fennici* **13**, 200–232 (1976).
9. E. Ranta, H. Lundberg, Resource partitioning in bumblebees: The significance of differences in proboscis length. *Oikos* **35**, 298–302 (1980).
10. L. D. Harder, Flower handling efficiency of bumble bees: Morphological aspects of probing time. *Oecologia* **57**, 274–280 (1983).
11. L. D. Harder, Effects of nectar concentration and flower depth on flower handling efficiency of bumble bees. *Oecologia* **69**, 309–315 (1986).
12. A. Lechantre, D. Michez, P. Damman, Collection of nectar by bumblebees: How the physics of fluid demonstrates the prominent role of the tongue's morphology. *Soft Matter* **15**, 6392–6399 (2019).
13. L. Shi, S. W. Nicolson, Y. Yang, J. Wu, S. Yan, Z. Wu, Drinking made easier: Honey bee tongues dip faster into warmer and/or less viscous artificial nectar. *J. Exp. Biol.* **223**, jeb229799 (2020).
14. D. W. Roubik, S. L. Buchmann, Nectar selection by *Melipona* and *Apis mellifera* (hymenoptera: Apidae) and the ecology of nectar intake by bee colonies in a tropical forest. *Oecologia* **61**, 1–10 (1984).
15. C. Zhao, J. Wu, S. Yan, Observations and temporal model of a honeybee's hairy tongue in microfluid transport. *J. Appl. Phys.* **118**, 194701 (2015).
16. J. Chen, J. Wu, S. Yan, Switchable wettability of the honeybee's tongue surface regulated by erectable glossal hairs. *J. Insect Sci.* **15**, 164 (2015).
17. C.-C. Li, J.-N. Wu, Y.-Q. Yang, R.-G. Zhu, S. Yan, Drag reduction effects facilitated by microridges inside the mouthparts of honeybee workers and drones. *J. Theor. Biol.* **389**, 1–10 (2016).
18. R. Zhu, H. Lv, T. Liu, Y. Yang, J. Wu, S. Yan, Feeding kinematics and nectar intake of the honey bee tongue. *J. Insect Behav.* **29**, 325–339 (2016).
19. C. Zhao, J. Wu, S. Yan, Erection mechanism of glossal hairs during honeybee feeding. *J. Theor. Biol.* **386**, 62–68 (2015).
20. Y. Yang, J. Wu, R. Zhu, C. Li, S. Yan, The honeybee's protrusible glossa is a compliant mechanism. *J. Bionic Eng.* **14**, 607–615 (2017).
21. H. Yang, J. Wu, S. Yan, Effects of erectable glossal hairs on a honeybee's nectar-drinking strategy. *Appl. Phys. Lett.* **104**, 263701 (2014).
22. H. Peisker, J. Michels, S. N. Gorb, Evidence for a material gradient in the adhesive tarsal setae of the ladybird beetle *Coccinella septempunctata*. *Nat. Commun.* **4**, 1661 (2013).
23. S. Gernay, W. Federle, P. Lambert, T. Gilet, Elasto-capillarity in insect fibrillar adhesion. *J. R. Soc. Interface* **13**, 20160371 (2016).
24. L. M. Sande, "Materials properties of the lepidopteran proboscis and a bio-inspired characterization method of capillary adhesion," Master's thesis, Clemson University, Clemson, SC (2017).
25. G. H. Pyke, N. M. Waser, The production of dilute nectars by hummingbird and honeyeater flowers. *Biotropica* **13**, 260–270 (1981).
26. T. Pamminger, R. Becker, S. Himmelreich, C. W. Schneider, M. Bergtold, The nectar report: Quantitative review of nectar sugar concentrations offered by bee visited flowers in agricultural and non-agricultural landscapes. *PeerJ* **7**, e6329 (2019).
27. W. Kim, T. Gilet, J. W. M. Bush, Optimal concentrations in nectar feeding. *Proc. Natl. Acad. Sci. U.S.A.* **108**, 16618–16621 (2011).
28. L. Landau, B. Levich, Dragging of a liquid by a moving plate. *Acta Physicochim. URSS* **17**, 42–54 (1942).
29. B. V. Derjaguin, On the thickness of the liquid film adhering to the walls of a vessel after emptying. *Acta Physicochim. URSS* **20**, 349–352 (1943).
30. B. V. Derjaguin, S. M. Levi, *Film Coating Theory* (The Focal Press, London, United Kingdom, 1964).
31. D. Quéré, Fluid coating on a fiber. *Annu. Rev. Fluid Mech.* **31**, 347–384 (1999).
32. A. Shimizu et al., Fine-tuned bee-flower coevolutionary state hidden within multiple pollination interactions. *Sci. Rep.* **4**, 3988 (2014).
33. J. Wu, R. Zhu, S. Yan, Y. Yang, Erection pattern and section-wise wettability of honeybee glossal hairs in nectar feeding. *J. Exp. Biol.* **218**, 664–667 (2015).
34. Y. Zhao, J. Wu, S. Yan, The morphology and reciprocation movement of honeybee's hairy tongue for nectar uptake. *J. Bionic Eng.* **13**, 98–107 (2016).
35. Z. He, W. Zhang, Y. Sun, C. Li, J. Wu, Z. Wu, How honey bees dip nectar: Dynamic spacing of tongue hairs facilitates to collect nectar of various viscosities. *J. Theor. Biol.* **512**, 110538 (2021).
36. M. Scherge, S. N. Gorb, *Biological Micro- and Nanotribology* (Springer-Verlag, Berlin, Germany, 2001).
37. C. Liao et al., Feeding behavior of honey bees on dry sugar. *J. Insect Physiol.* **124**, 104059 (2020).
38. L. D. Landau, E. M. Lifshitz, *Theory of Elasticity* (Pergamon Press, New York, NY, ed. 3, 1986).
39. F. M. White, *Fluid Mechanics* (McGraw-Hill, New York, NY, ed. 7, 2011).
40. H. Lamb, On the uniform motion of a sphere through a viscous fluid. *Lond. Edinb. Dubl. Phil. Mag.* **21**, 112–121 (1911).
41. M. Mathlouthi, J. Génotelle, "Rheological properties of sucrose solutions and suspensions" in *Sucrose—Properties and Applications*, M. Mathlouthi, P. Reiser, Eds. (Blackie Academic and Professional, London, United Kingdom, 1995), pp. 126–154.
42. R. Saggin, J. N. Coupland, Rheology of xanthan/sucrose mixtures at ultrasonic frequencies. *J. Food Eng.* **65**, 49–53 (2004).
43. M. Quintas, T. R. S. Brandão, C. L. M. Silva, R. L. Cunha, Rheology of supersaturated sucrose solutions. *J. Food Eng.* **77**, 844–852 (2006).
44. D. Bierman, W. H. Herrnstein, "The interference between struts in various combinations" (Tech. Rep. 468, National Advisory Committee for Aeronautics, Washington, DC, 1933).
45. P. W. Bearman, A. J. Wadcock, The interaction between a pair of circular cylinders normal to a stream. *J. Fluid Mech.* **61**, 499–511 (1973).
46. V. Aroulmoji, V. Aguié-Béghin, M. Mathlouthi, R. Douillard, Effect of sucrose on the properties of caffeine adsorption layers at the air/solution interface. *J. Colloid Interface Sci.* **276**, 269–276 (2004).
47. D. P. Cariveau et al., The allometry of bee proboscis length and its uses in ecology. *PloS One* **11**, e0151482 (2016).
48. S. G. T. Klumpers, M. Stang, P. G. L. Klinkhamer, Foraging efficiency and size matching in a plant–pollinator community: The importance of sugar content and tongue length. *Ecol. Lett.* **22**, 469–479 (2019).
49. M. A. Peuker et al., Floral traits are associated with the quality but not quantity of heterospecific stigmatic pollen loads. *BMC Ecol.* **20**, 54 (2020).

Lechantre et al.
Essential role of papillae flexibility in nectar capture by bees

PNAS | 7 of 7
https://doi.org/10.1073/pnas.2025513118